Available online at www.sciencedirect.com

ScienceDirect

journal homepage: www.elsevier.com/locate/he

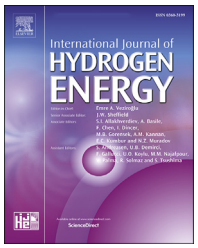

Improved ball milling method for the synthesis of nanocrystalline TiFe compound ready to absorb hydrogen

L.E.R. Vega [a], *D.R. Leiva* [a], *R.M. Leal Neto* [b,*], *W.B. Silva* [a], *R.A. Silva* [a], *T.T. Ishikawa* [a], *C.S. Kiminami* [a], *W.J. Botta* [a]

[a] *Federal University of São Carlos - UFSCar, Rod. Washington Luis, Km 235, CEP 13565-905, São Carlos, SP, Brazil*
[b] *Energy and Nuclear Research Institute (IPEN), Av. Prof. Lineu Prestes, 2242 Cidade Universitária, CEP 05508-000, São Paulo, SP, Brazil*

HIGHLIGHTS

- As-milled TiFe absorbs hydrogen at room temperature requiring no thermal activation.
- High yields were obtained by preparing the media surfaces previously.
- Mechanical alloyed TiFe milled for 6 h absorbed 1 wt% of hydrogen at 20 bar.
- Jander model best fits the first hydrogenation of samples milled for 2 h and 6 h.

ARTICLE INFO

Article history:
Received 5 June 2019
Received in revised form
11 October 2019
Accepted 6 November 2019
Available online 4 December 2019

Keywords:
Mechanical alloying
Ball milling
Hydrogen storage
TiFe
Hydrides
Activation

ABSTRACT

In this study, we propose a method to produce nanocrystalline TiFe powder by high-energy ball milling, in order to avoid the common sticking problem of the material to the milling tools, assuring a material prompt to absorb hydrogen as well. The method consists of making a preliminary milling operation with the elemental powders (50:50 stoichiometric ratio) to form a strong adhered layer of the milled material on the surfaces of the vial and balls. The main milling operation is then performed with a new powder charge (same composition as before), but now adding a process control agent (stearic acid). Various processing times - 2, 6, 10 and 20 h - were used in the milling experiments. Nanocrystalline TiFe was synthesized in this way with low oxygen contamination, full yields for milling times of 6 h or over, requiring no heat treatments for the first hydrogen absorption. Hydrogen storage capacity of 1.0 wt% at room temperature under 20 bar was attained by the sample milled for 6 h. Kinetic data from samples milled for 2 h and 6 h agreed with Jander model for the rate limiting step of the hydriding reaction, which is based on diffusion with constant interface area.

* *Corresponding author.*
E-mail address: lealneto@ipen.br (R.M. Leal Neto).
https://doi.org/10.1016/j.ijhydene.2019.11.035

Introduction

Hydride-forming metals or alloys are considered the safest way to storage hydrogen, compared to high pressure or cryogenic tanks. Among them, TiFe intermetallic compound, has been considered as hydrogen storage material since the earlier 1970s [1,2]. TiFe reacts reversibly with hydrogen at room temperature to form two AB-type hydrides, TiFeH and $TiFeH_2$, with theoretical gravimetric storage capacities 0.96 wt % and 1.91 wt%, respectively. Such capacities combined with the low price of components justify the continuous investigations on this material. Research has been concentrated on solving problems related to the formation of a passive oxide layer on its surface, impairing hydrogen entrance. An activation procedure is necessary to the first hydrogen absorption, particularly when TiFe is produced by melting, or even reactivated when previously activated TiFe is exposed to oxygen.

Activation can be accomplished by various manners that are classified in three groups: thermal, chemical and mechanical activation. Whatever the group, the main intention is to make the first hydrogenation easier and to improve kinetics and/or capacity. Thermal activation is the most traditional and frequent way and consists of long and complex heat treatment cycles, e.g., heating under high vacuum levels and cooling under high hydrogen pressures [2–6]. Chemical activation consists of adding other elements to the TiFe alloy, like Ce [7], Co [8], Cr [9], Cu [10], Mn [11], Nb [12], Ni [13], V [14] and Zr [15], or even changing the stoichiometry of the intermetallic [16,17]. Mechanical activation comprises different processing techniques, based on the increase of the density of defects (nanocrystalline structure) and/or surface area: ball milling [18–38], cold rolling [39,40] and severe plastic deformation [41,42]. Two different process routes have been adopted to obtain TiFe powder by ball milling: mechanical alloying of a mixture from the elemental powders [18–23,25,28,30,31,35,37] and mechanical grinding of pre-melted and homogenized TiFe compound or alloy [22,27,29,30,32,34,36,43].

This study deals with mechanical alloying of TiFe performed by high-energy ball milling (HEBM). Mechanical alloying is a solid-state process based on successive welding and fracture of the elemental powder particles that takes place under high energetic impact of the balls to the vial's walls and between each other. Several variables influence the process and must be taken in account to get reproducible results, like type of mill, ball to powder mass ratio, ball and vial size, ball and vial material, time and atmosphere of milling [44,45]. Ductile metal powder particles plastically deform and exhibit strong tendency to weld each other (which is vital for the alloying process). At the same time, they exhibit also a strong tendency to stick on the surface of the vial and balls. It is imperious for mechanical alloying success to control this stick tendency of the particles, assuring a good yield in terms of loose powder mass effectively available after milling.

Despite that, this very common problem of sticking of TiFe on the milling vial and balls is only barely reported. Abe et al. [31], for example, correlated the better yield (collecting efficiency, as called by them) with the existence of the amorphous TiFe phase. After milling for 15 h (more crystalline state) and 20 h (more amorphous phase) they got yields of about 9% and 96%, respectively. Thus, they decide to mill for only 5 h (85% yield, but incomplete alloying) and perform a post-annealing treatment to produce almost 100% TiFe alloy. Falcão et al. [23] have performed the mechanical alloying of TiFe in a shaker mill using different organic PCAs (Process Control Agents), like ethanol, stearic acid, low density polyethylene, benzene and cyclohexane. Cold welding and sticking can be controlled by addition of PCAs. It was seen by those authors that massive cold welding could only be prevented by adding higher amounts of PCAs (10 wt% or over), which impairs the alloying and the formation of the compound. The higher the amount of PCA, particularly benzene and cyclohexane, longer the time of milling to form TiFe phase, but only partially, since TiC was also formed as result from the decomposition of the PCAs during prolonged milling operation. Considering the sticking pattern of the cold-welded material, which is rather concentrated in a part of the vial, they decided to conduct further milling operation in a planetary ball mill and use titanium hydride instead of Ti with Fe powder as starting material [28] and got over 95% of yield. After a post-annealing treatment, nanocrystalline TiFe was obtained ready to absorb hydrogen.

Emami et al. [27] performed mechanical milling of TiFe in a planetary mill using about 20 wt% of acetone as process control agent, but the yield was not reported. The use of acetone was apparently responsible for the contamination with 11 at.% of oxygen and 8 at.% of carbon in the milled samples. López-Baéz et al. [20] employed an interesting method to bypass the problems with contamination from the vial and balls when performing mechanical alloying of TiFe. This method will be described here, since it has inspired us to make the present work. Before each grinding, the walls of the vial and the surface of the balls were covered with both Ti and Fe powders, at the same proportion related to the desired formulation (50:50 in this case). This was done by previously grinding a small amount of powders for a few hours, after observing that this powder adhered to the internal surface of the grinding medium. This adherence was not complete however, since the authors reported that all non-adhered material was removed, before the main grinding was started with a new powder charge. Besides not specifying the amount of powders, the authors have not reported the type of mill device they used. By the way, some lack of information on the published articles for this system is the general rule, which impairs the attempts to reproduce the results, an essential matter of scientific investigations.

The main objective of this study was to synthesize TiFe compound by mechanical alloying following a process strategy that accomplish a good milling yield (related to the sticking issue), by preliminary grinding of the Ti and Fe powders, producing a material prone to absorb hydrogen and with good storage properties.

Experimental

Ti (−100 mesh, 99.4%) and Fe (−20 mesh, 99%) elementary powders were weighed at the 50:50 stoichiometric ratio and placed in a milling vial (AISI 450 - 1% C-3 Cr ferritic steel, 500

Table 1 – Yields after each milling batch.

Milling time (h)	Yield[a] (wt. %)	Amount of loose powder (grams)
2	33	0.67
6	120	2.43
10	120	2.43
20	120	2.43

[a] excluding initial powder mass for surface preparation of the vial and balls.

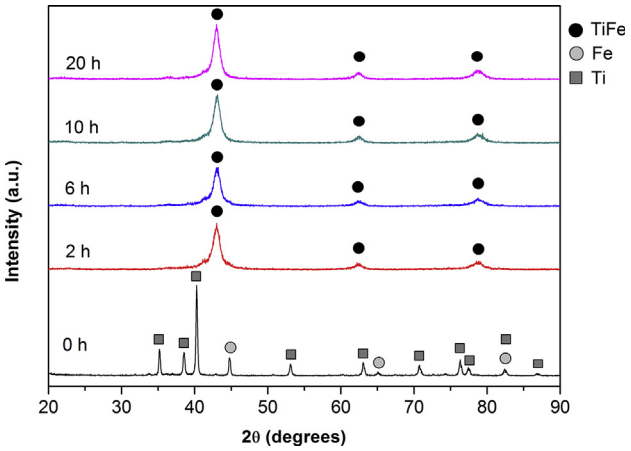

Fig. 1 – XRD patterns of the as-milled samples (times of milling are indicated).

Table 2 – EDS analysis of milled TiFe particles.

Milling time	Element (at. %)	
	Ti	Fe
2 h	49.5 ± 1.4	50.5 ± 1.4
6 h	50.3 ± 0.1	49.7 ± 0.1

HB, inner volume of 160 ml) with chrome steel balls (10 balls with 10 mm diameter and 15 balls with 8 mm diameter). The ball to material mass ratio was 40:1. All experiments were performed in a planetary mill (Fritsch Pulverisette 6) at a speed of 600 rpm under an atmosphere of 3 bar of argon. A special vial was designed and built to allow pressurization.

Initially a pre-milling operation of the elementary powders (2 g) was performed to prepare superficially the vial and balls, creating a TiFe layer with minimal oxidation. This was done until all the material was fully adhered to the vial's walls and balls' surfaces, which was accomplished after 6 h. Thus, Ti and Fe powders were charged again (2 g), this time with 1.5 wt % of the stearic acid (0.03 g), added as process control agent. The powder mixture was then milled individually for various times (2, 6, 10 and 20 h). Each batch (run) was started with clean vial and media, followed by the pre-milling operation as described. Milling yields were calculated based on the loose powder mass extracted from the vial related to the main (second) charge mass (2.03 g), i.e., excluding the powder mass used in the pre-milling operation.

The handling of the elemental powders before and after each milling run was carried out within a glovebox (MBRAUN

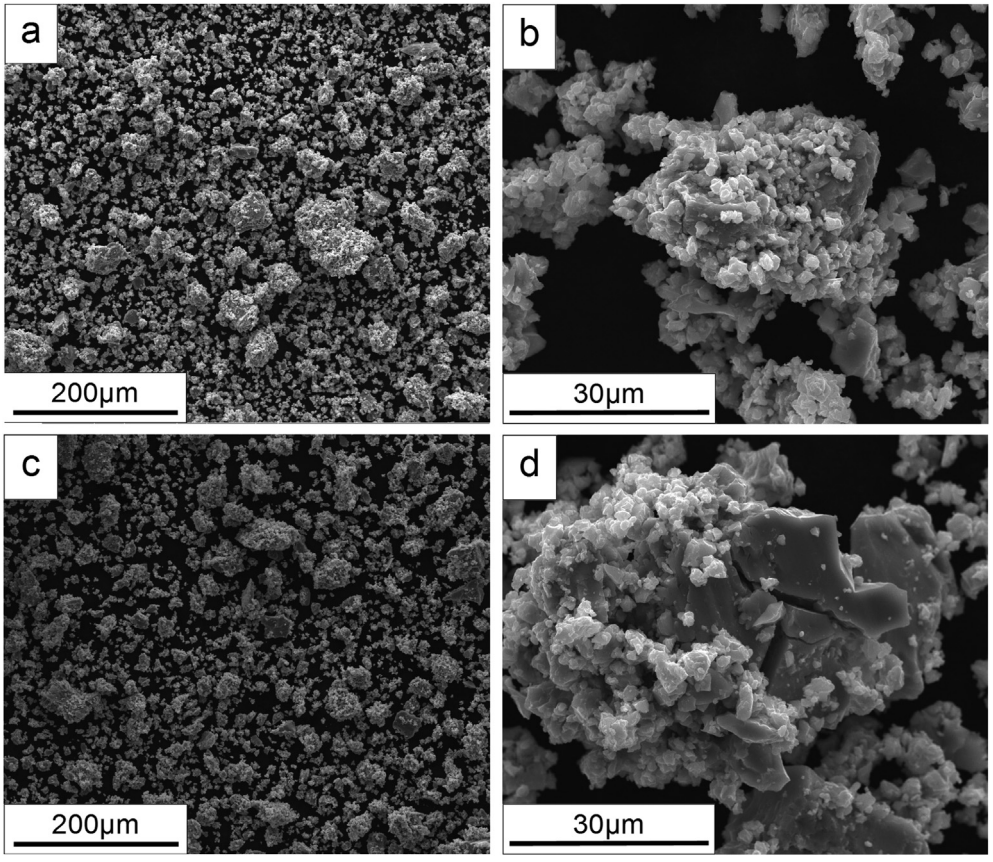

Fig. 2 – SEM images (secondary electrons) of TiFe particles after milling for 2 h (a,b) and 6 h (c,d).

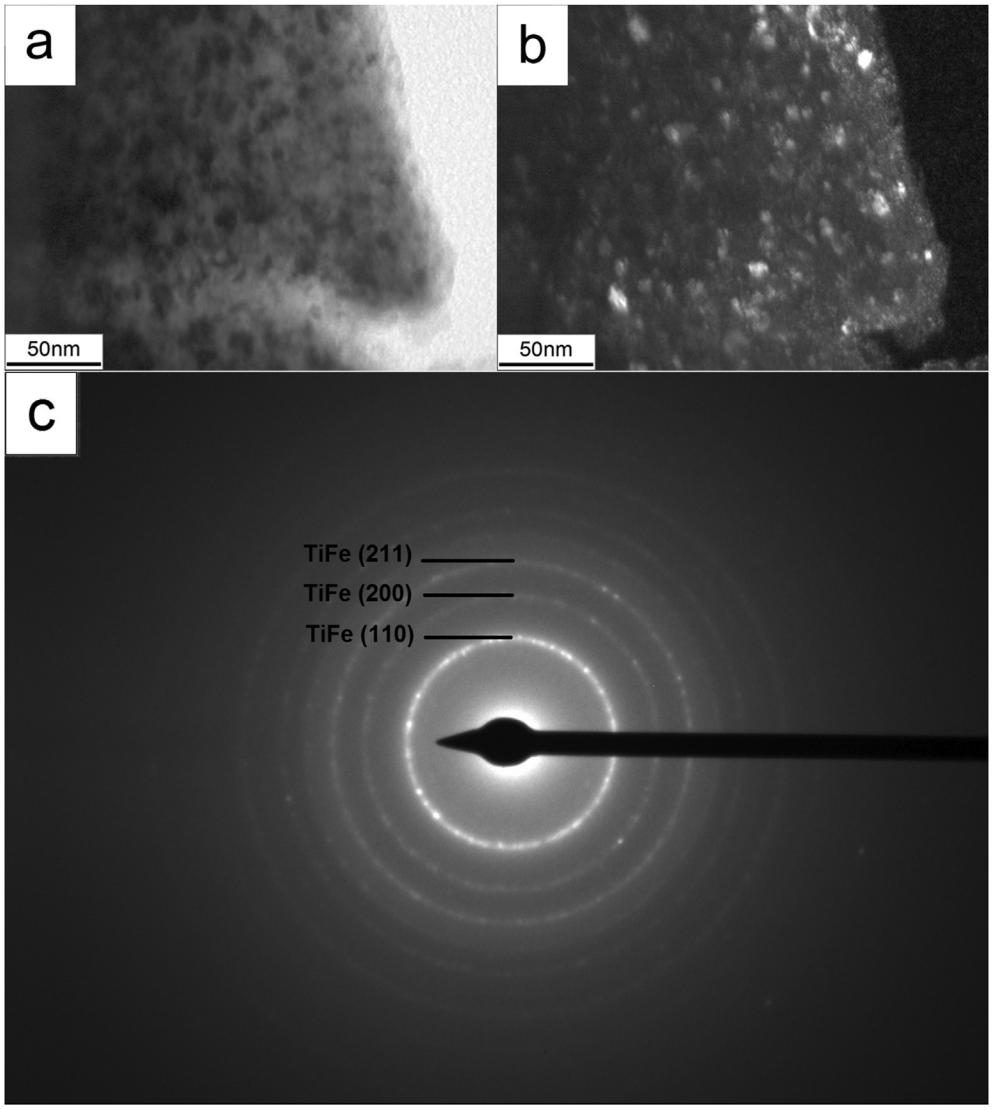

Fig. 3 – TEM images of TiFe powder milled for 2 h: (a) Bright field image; (b) dark field image from diffraction ring corresponding to (110) planes; (c) electron diffraction pattern.

LAB Master 130) under purified argon (close circuit), with H_2O and O_2 levels below 0.1 ppm to reduce contamination. Samples before and after milling were analyzed by X-ray diffraction (XRD) with Cu-Kα radiation at 40 kV and 40 mA in a Siemens D 5005 diffractometer. The mean crystallite size of the milled samples was estimated using the Scherrer equation, according to the method described in Ref. [45]. Scanning electron microscopy (SEM) analyses were conducted on an Inspect microscope equipped with an energy dispersive X-ray spectroscopy (EDS) detector. Transmission electron microscopy (TEM) analyses were accomplished in a high resolution TEM from FEI TECNAI G^2 F20. The oxygen content and specific surface area of the milled samples were measured by inert gas fusion technique (ONH836 elemental analyzer from LECO) and nitrogen physisorption (ASAP 2020 from Micromeritics), respectively. Three measurements per sample were conducted. In order to minimize possible oxygen contamination of the samples in their transport from the glovebox to the oxygen content analyzer, they were loaded, still in the glovebox, in the analytical crucible, and then placed inside a hermetic pot.

Hydrogen storage properties were evaluated at room temperature under 20 bar H_2 pressure using a homemade Sieverts volumetric apparatus. Samples milled and exposed to atmospheric air also had their H_2 absorption properties measured and compared with the non-exposed samples to evaluate their oxidation or air resistance.

Results and discussion

After pre-milling for 6 h, the adhered material on the vial and balls was so strong welded that no powder can be removed easily by a gentle brushing. No loose powder was observed as

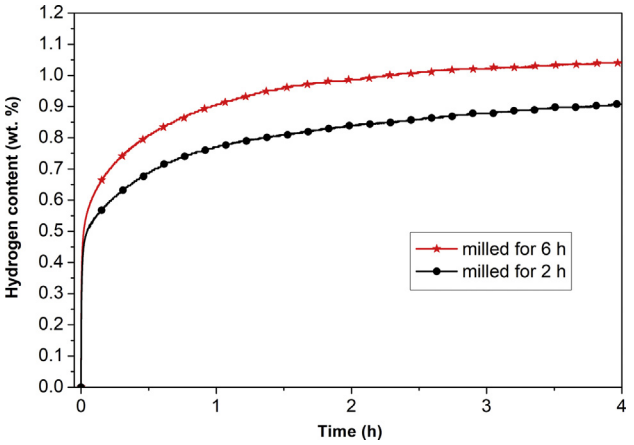

Fig. 4 – Room temperature kinetics for the first hydrogen absorption (20 bar) of the as-milled samples (not thermally activated).

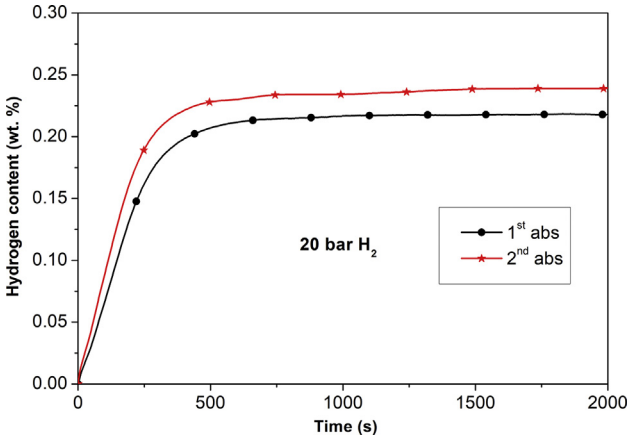

Fig. 5 – Hydrogen absorption kinetic curves of the TiFe sample milled for 6 h after 5 h of air-exposure and application of thermal activation.

well, so we considered this covering strategy successful. Table 1 shows the yields after main milling operation for each time batch (2, 6, 10 and 20 h). For clarity purposes the amount of loose powder after milling was also given.

After milling for 2 h poor yield was noticed (33%), apparently indicating that the amount of PCA was not enough to avoid the sticking of the main charge to the previous material of the covering layer. Surprisingly, milling for 6 h yields 120%, which kept unchanged for 10 and 20 h of milling. Regarding this, some observations can be made:

1 some material was detached from the covering layer, as indicated by the yields over 100%;
2 The time of the detachments were unknown, so there is some uncertainty about the effective milling time of the detached material;
3 It seems that a kind of equilibrium between detachment and adherence of particle was attained after milling for 6 h;
4 The yields obtained here are higher than previous reported ones, under 100% [28,31].

XRD patterns of samples before and after milling are shown in Fig. 1. TiFe compound (simple cubic CsCl-type structure) was completely formed after milling for 2 h. Diffraction patterns are quite the same after milling for 2, 6, 10 and 20 h. The mean crystallite size, estimated from the peak broadening (Scherrer formula), remained around 10 nm in all milled samples, confirming the similarity of the patterns shown in Fig. 1. This crystallite size is compatible with the ones previously repported for mechanical alloyed TiFe in planetary ball mills [25,27]. The results indicate that a saturation of the crystallite size refinement for the TiFe compound is attained after 2 h of milling. We believe that the higher ball to powder mass ratio (40:1), the size of the balls (10 mm) and the rotation speed (600 rpm) used in the experiments can explain this behavior, compared to other experiments with planetary ball milling [18,19,24,25,27,28,35]. Reported ball to powder mass ratios range from 4:1 [27] to 20:1 [28,35]. Chu et al. [18] used large balls (12.7 mm), but with the intention to obtain amorphous TiFe. Zadorozhnyy et al. [25] used higher rotation speed (840 rpm) but both smaller balls (4 mm) and ball to powder ratio (10:1), attaining a crystallite size similar to the present work after 2 h of milling. Therefore, further results will be focused on samples milled for 2 and 6 h only.

Fig. 2 shows SEM micrographs (secondary electrons) of the mechanical alloyed TiFe particles milled for 2 and 6 h. There are two populations concerning the particle size: one is composed by very fine particles under 10 μm many that forms agglomerates; other is composed by very large cracked particles, surrounded by the fine ones, that can be better seen in Fig. 2d. Regarding the former discussion, we believe that small particles are formed from the mechanical alloying with stearic acid (main charge) and the others came from detachment of

Table 3 – Surface area and gas content (O and N) of TiFe samples.

Milling time (h)	Surface area (m^2g^{-1})	O (wt. %)	N (wt. %)
2	0.466	0.313 ± 0.007	0.082 ± 0.002
6	0.725	0.316 ± 0.001	0.089 ± 0.001
6 (after air exposure for 5 h)	–	0.709 ± 0.002	0.085 ± 0.001

Table 4 – Reported values of hydrogen absorption capacities compared with this study.

Milling time	Absorption conditions	wt. % H_2	Reference
2 h	295 K, 400 bar	1.4	[25]
10 h	295 K, 50 bar	1.09	[31]
2 h	295 K, 40 bar	1.35	[25]
2 h	295 K, 20 bar	~1.0	[25]
2 h	308 K, 60 bar	~1.0	[46]
20 h	298 K, 250 bar	1.3	[21]
36 h	303 K, ~80 bar	1.5	[27]
38 h	Room temperature, ~27 bar	~1.1	[30]
40 h	Room temperature, 19 bar	0.94	[28]
90 h	298 K, 50 bar	~1.3	[22]
2 h	Room temperature, 20 bar	0.9	**This work**
6 h	Room temperature, 20 bar	1.0	**This work**

Table 5 – Equations used for fitting experimental sorption data [49–52] along with calculated R^2 coefficients from the absorptions curves of samples milled for 2 h and 6 h (α is the reacted fraction as defined in the text).

Model equation (integral form)	Kinetic model designation and description	R^2	
		2 h	6 h
$\alpha = kt$	Chemisorption: surface controlled	0.79195	0.73447
$[-\ln(1-\alpha)]^{1/3} = kt$	JMA-3D: Johnson-Mehl-Avrami, three-dimensional growth of existing nuclei with constant interface velocity	0.95601	0.95211
$[-\ln(1-\alpha)]^{1/2} = kt$	JMA-2D: Johnson-Mehl-Avrami, two-dimensional growth of existing nuclei with constant interface velocity	0.96931	0.96795
$1-[1-\alpha]^{1/3} = kt$	CV-3D: contracting volume, three-dimensional growth with constant interface velocity	0.96168	0.94904
$1-(1-\alpha)^{1/2} = kt$	CV-2D: contracting volume, two-dimensional growth with constant interface velocity	0.93123	0.90663
$1-(2\alpha/3)-(1-\alpha)^{2/3} = kt$	GB-3D: Ginsling-Braunshteinn, three-dimensional growth (sphere), diffusion controlled with decreasing interface velocity	0.96864	0.94527
$(1-\alpha)\ln(1-\alpha)+\alpha = kt$	GB-2D: Ginsling-Braunshteinn, two-dimensional growth (cylinder), diffusion controlled with decreasing interface velocity	0.93849	0.90054
$[1-(1-\alpha)^{1/3}]^2 = kt$	Jander: constant volume, diffusion controlled with constant diffusion interface area	0.99213	0.99203

the covering layer (pre-milling). The action of the PCA during mechanical alloying controls the welding between the particles and results in finer particles [45], so it is reasonable to think that particles from the main charge are smaller than the ones produced without the additive.

Chemical composition of the HEBM samples (2 and 6 h) were determined by microanalysis (EDS) and is presented in Table 2. Ti and Fe contents are in agreement with the expected values with no significant deviations.

Fig. 3 shows TEM images of a TiFe particle after milling for 2 h. The microstructure of the sample exhibits crystallites, whose size is compatible with the one estimated by XRD analysis (10 nm) and from those previously reported in the literature [21,27,46].

Hydrogen absorption kinetic curves of as-milled TiFe samples (2 and 6 h), measured at room temperature under 20 bar H_2, are shown in Fig. 4.

After 4 h, the hydrogen storage capacity of samples milled for 2 h and 6 h reached about 0.9 wt% and 1 wt%, respectively. It should be emphasized that samples were not heat treated (no thermal activation). Moreover, sample milled for 6 h showed a faster absorption kinetics than the sample milled for 2 h. The higher kinetics and capacity could be explained first with the help of specific surface area analysis shown on Table 3. Although both powders have low surface areas, the area of the sample milled for 6 h is 56% higher. Second, since there were no heat treatments before the first hydrogenation, stearic acid could impair absorption. We should expect some volatilization or even decomposition during the milling operation. Whatever the case, the sample milled for 2 h has probably more stearic acid content than the sample milled for 6 h which could explain its lower capacity.

It is important to mention that in the available literature on hydrogen storage properties of TiFe processed by mechanical alloying, there is much more information on pressure-composition isotherms (PCI curves, equilibrium pressure x hydrogen content) [4,10,11,13,14,19] than on kinetic curves [22]. Table 4 compares the values of hydrogen absorption capacities from the PCI curves found in literature with the results of this study.

Higher absorption capacities were reached (>1 wt%) when higher pressures were used. With similar pressure range, our data are similar to the previous ones. Most references from Table 4 [21,22,25,27,30,31] reported the need to perform a thermal activation (or reactivation) after milling to provide the first hydrogen absorption. In the present work, as-milled samples reacted readily upon contact with hydrogen. The pre-milling operation for surface preparation (vial and balls), protected the material from oxygen contamination of the vessel walls and the surface of the balls, as indicated by the low oxygen contents shown in Table 3. These values are much lower than those presented in previous research [30,46], which means that we could synthesize a more clean and reactive material. On the other hand, care with the milling atmosphere is also a relevant aspect for the TiFe hydrogen absorption/desorption properties. It has been reported that if Ti and Fe elements are processed by high energy milling at an oxygen content greater than 3 at.%, some amorphous TiFe is generated [30], which impairs hydrogenation, requiring a thermal activation after milling [18]. In the present study we did not have such problems.

Emami et al. have reported that mechanical alloyed TiFe can exhibit a good air resistance, even after ~1 month of air exposure [27]. In the present work the sample milled for 6hs was left in air for just 5 h. This time, the kinetic curves was determined for the first and the second hydrogen absorption (Fig. 5). The exposed milled material absorbed less than 0.3 wt % of hydrogen after 2000s, compared with about 0.8% from the sample not exposed to air after the same time. The increased oxygen content after air exposure (Table 3) can explain this deterioration, a well-known problem of TiFe [33,46–48], not confirming of what was observed by Emami et al. [27]. In that case, maybe the carbide contamination (resulted from the high content of acetone used as PCA) could avoid the continuity of the oxide layer on the surface of TiFe particles, which allowed the hydrogen atoms entrance after 1 month of air

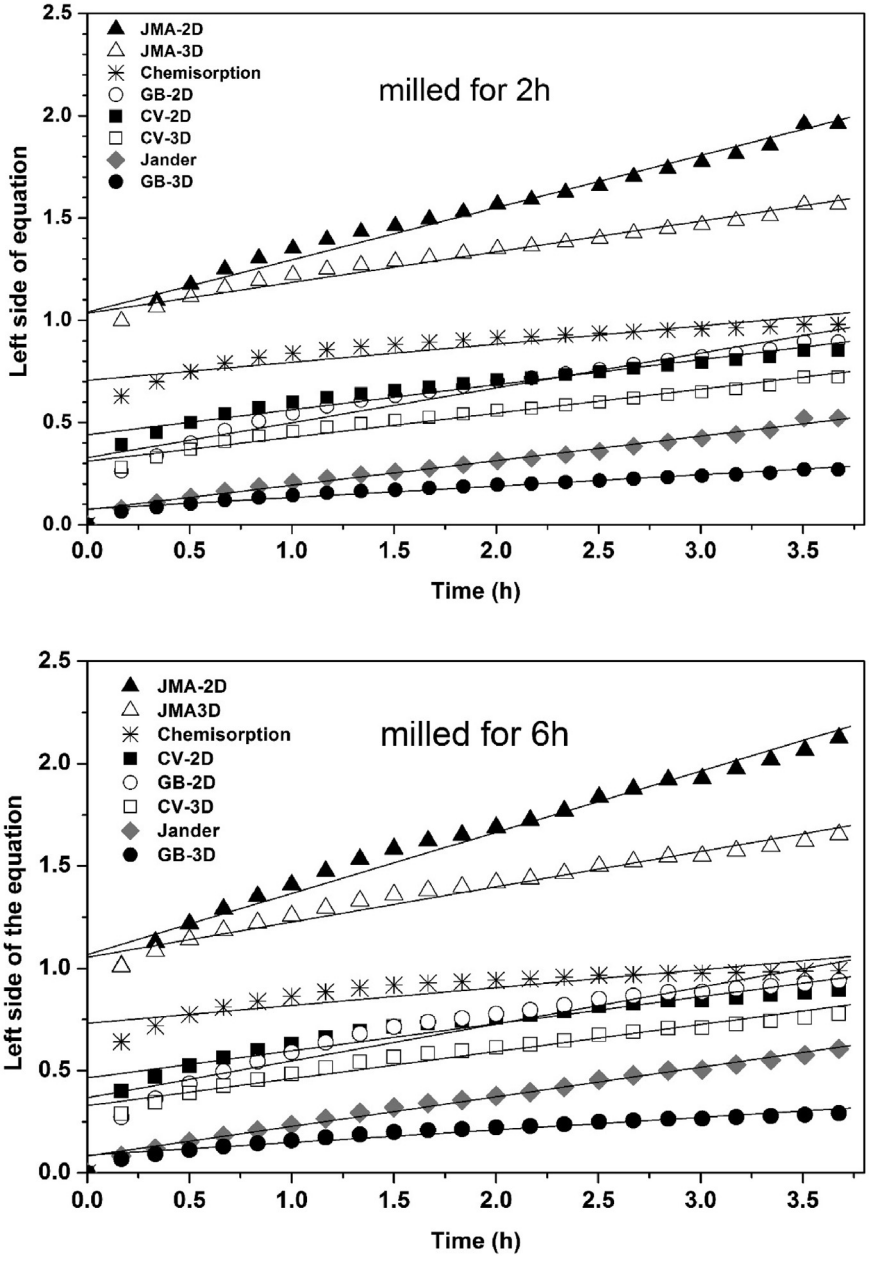

Fig. 6 – Linear fitting of the rate limiting step models for the first hydrogenation of milled samples.

exposure and after a heat treatment (423 K for 2 h under mechanical vacuum) before the PCI measurements.

We have used the experimental kinetic absorption curves from Fig. 4 to identify the rate-limiting step of the hydriding reaction in mechanical alloyed TiFe powders. The slowest step can be deduced by fitting experimental data with the analytical expression of the various kinetic models [49–52]. The best fitted model will indicate the most probable limiting step. A very common and easiest procedure to find this out is to arrange the model equations by leaving in the left side a function of the reacted fraction α, that ranges from 0 (at the beginning of the reaction) to 1 (maximum attained capacity). The right side of all equations will be kt, where k is the reaction constant and t is the reaction time. The best fitted model will give then a straight line and the fitness quality can be measured by the squared correlation coefficient R^2, calculated in the regression by the least squares method. Table 5 reports the models tested here.

It is worth to say that very powerful Chou model [53–56] relating to surface penetration of hydrogen atoms controlled and diffusion of hydrogen controlled is not tested here. It is mathematically equivalent to the CV-2D (surface penetration controlled) and Jander (diffusion controlled) models, with the rate constant k expressed as $1/tc_{(sp)}$ and $1/tc_{(d)}$, respectively. Here $tc_{(sp)}$ and $tc_{(d)}$ are the "characteristic-reaction times", controlled by surface penetration (sp) and diffusion (d), both representing the required time for full hydriding reaction.

Linear fitting curves are shown in Fig. 6 for the samples milled for 2 h and 6 h. It can be seen that Jander model [57], despite its alleged limitations (such as the constant diffusion

interface area), was by far the model that best suited the experimental data from both samples. Thus, the rate limiting step, as suggested by the results, has not changed with the milling time, so the faster kinectics from sample milled for 6 h can be attributed only to the increased mechanical activation.

Previous investigations on kinetc models were conducted on TiFe, but with additions of Zr [58] or Zr plus V [59]. In both cases GB-3D model was best fitted to the data, but Jander model was not considered.

Conclusions

Mechanical alloying of TiFe by high energy ball milling was successfully accomplished regarding the yield and the ability to absorb hydrogen of the as-milled material, not requiring thermal activation. To do so, we have performed a preliminary milling of Ti and Fe powders aiming to covering the surfaces of the vial and the media with a strong adhered layer of the milled material. After that a new charge of the elemental powders was milled, this time with stearic acid, assuring excellent yields after 6 h of milling and producing clean nanocrystalline TiFe compound (low oxygen contamination), ready to absorb about 1 wt % of hydrogen at room temperature (20 bar). Jander model, based on diffusion controlled with constant diffusion interface area, best fits the experimental data from both samples.

Acknowledgments

The authors would like to thank FAPESP (grant number 2013/05987-8), CAPES and CNPq for the financial support.

REFERENCES

[1] Wiswall RHJ, Reilly JJ. Metal hydrides for energy storage. San Diego: 7th. Intersoc. energy Convers. Eng. Conf.; 1972. p. 1–22.
[2] Reilly JJ, Wiswall RH. Formation and properties of iron titanium hydride. Inorg Chem 1974;13:218–22. https://doi.org/10.1021/ic50131a042.
[3] Schlapbach L, Riesterer T. The activation of FeTi for hydrogen absorption. Appl Phys A Solids Surfaces 1983;32:169–82. https://doi.org/10.1007/BF00820257.
[4] Kim HC, Lee J. A study on the activation mechanism of FeTi in view of surface conditions of metals. Int J Hydrogen Energy 1985;10:543–5. https://doi.org/10.1016/0360-3199(85)90085-0.
[5] Ma J, Pan H, Wang X, Chen C, Wang Q. Hydrogen storage properties of $FeTi_{1.3+x}$ wt%Mm (x=0.0, 1.5, 3.0, 4.5, 6.0) hydrogen storage alloys. Int J Hydrogen Energy 2000;25:779–82. https://doi.org/10.1016/S0360-3199(99)00100-7.
[6] Ali W, Hao Z, Li Z, Chen G, Wu Z, Lu X, et al. Effects of Cu and Y substitution on hydrogen storage performance of $TiFe_{0.86}Mn_{0.1}Y_{0.1-x}Cu_x$. Int J Hydrogen Energy 2017;42:16620–31. https://doi.org/10.1016/j.ijhydene.2017.04.247.
[7] Leng H, Yu Z, Yin J, Li Q, Wu Z, Chou K-C. Effects of Ce on the hydrogen storage properties of $TiFe_{0.9}Mn_{0.1}$ alloy. Int J Hydrogen Energy 2017;42:23731–6. https://doi.org/10.1016/j.ijhydene.2017.01.194.
[8] Boulghallat M, Gerard N. Hydriding kinetics of $TiFe_{0.5}Co_{0.5}$ compounds. J Less Common Met 1991;172–174:1052–7. https://doi.org/10.1016/S0022-5088(06)80011-1.
[9] Lee S-M, Perng T-P. Effect of the second phase on the initiation of hydrogenation of $TiFe_{1-x}M_x$ (M = Cr,Mn) alloys. Int J Hydrogen Energy 1994;19:259–63. https://doi.org/10.1016/0360-3199(94)90095-7.
[10] Ali W, Li M, Gao P, Wu C, Li Q, Lu X, Li C. Hydrogenation properties of Ti-Fe-Mn alloy with Cu and Y as additives. Int J Hydrogen Energy 2017;42:2229–38. https://doi.org/10.1016/j.ijhydene.2016.09.037.
[11] Chung H, Lee J. Hydriding and dehydriding reaction rate of FeTi intermetallic compound. Int J Hydrogen Energy 1985;10:537–42. https://doi.org/10.1016/0360-3199(85)90084-9.
[12] Fukushima S, Tanabe H. Surface properties of TiFe and TiFe-Nb 6.8 at.% electrodes in aqueous solution. Int J Hydrogen Energy 1983;8:33–7. https://doi.org/10.1016/0360-3199(83)90032-0.
[13] Chung HS, Lee JY. Effect of partial substitution of Mn and Ni for Fe in FeTi on hydriding kinetics. Int J Hydrogen Energy 1986;11:335–9. https://doi.org/10.1016/0360-3199(86)90153-9.
[14] Guéguen A, Latroche M. Influence of the addition of vanadium on the hydrogenation properties of the compounds $TiFe_{0.9}V_x$ and $TiFe_{0.8}Mn_{0.1}V_x$ (x = 0, 0.05 and 0.1). J Alloy Comp 2011;509:5562–6. https://doi.org/10.1016/j.jallcom.2011.02.036.
[15] Patel AK, Sharma P, Huot J. Effect of annealing on microstructure and hydrogenation properties of TiFe + X wt % Zr (X = 4, 8). Int J Hydrogen Energy 2018;43:6238–43. https://doi.org/10.1016/j.ijhydene.2018.02.029.
[16] Mizuno T, Morozumi T. Titanium concentration in $FeTi_x$ ($1 \leqslant x \leqslant 2$) alloys and its effect on hydrogen storage properties. J Less Common Met 1982;84:237–44. https://doi.org/10.1016/0022-5088(82)90148-5.
[17] Lee SM, Perng TP. Microstructural correlations with the hydrogenation kinetics of $FeTi_{1+x}$ alloys. J Alloy Comp 1991;177:107–18. https://doi.org/10.1016/0925-8388(91)90061-.
[18] Chu B, Lee S, Perng T. Preparation and hydrogen absorption property of amorphous $Ti_{50}Fe_{50}$. Int J Hydrogen Energy 1991;16:413–6. https://doi.org/10.1016/0360-3199(91)90141-5.
[19] Eckert J, Schultz L, Urban K. Synthesis of NiTi and FeTi alloys by mechanical alloying: formation of amorphous phases and extended solid solutions. J Non-Cryst Solids 1991;127:90–6. https://doi.org/10.1016/0022-3093(91)90404-T.
[20] López-Báez I, Espinoza-Beltrán FJ, Barreiro-Rodríguez G. Desarrollo de un nanomaterial base TiFe, como electrode para baterías recargables tipo NiMH, obtenido por aleado mecánico de alta energía. Rev Mex Fis 2006;52:278–84.
[21] Hotta H, Abe M, Kuji T, Uchida H. Synthesis of Ti-Fe alloys by mechanical alloying. J Alloy Comp 2007;439:221–6. https://doi.org/10.1016/j.jallcom.2006.05.137.
[22] Haraki T, Oishi K, Uchida H, Miyamoto Y, Abe M, Kokaji T, Uchida S. Properties of hydrogen absorption by nano-structured FeTi alloys. Int J Mater Res 2008;99:507–12. https://doi.org/10.3139/146.101669.
[23] Falcão RB, Dammann EDCC, Rocha CJ, Leal Neto RM. An investigation on the mechanical alloying of TiFe compound by high-energy ball milling. Mater Sci Forum 2010;660–661:329–34. https://doi.org/10.4028/www.scientific.net/MSF.660-661.329.

[24] Abrashev B, Spassov T, Bliznakov S, Popov A. Microstructure and electrochemical hydriding/dehydriding properties of ball-milled TiFe-based alloys. Int J Hydrogen Energy 2010;35:6332–7. https://doi.org/10.1016/j.ijhydene.2010.03.129.
[25] Zadorozhnyy V, Klyamkin S, Zadorozhnyy M, Bermesheva O, Kaloshkin S. Hydrogen storage nanocrystalline TiFe intermetallic compound: synthesis by mechanical alloying and compacting. Int J Hydrogen Energy 2012;37:17131–6. https://doi.org/10.1016/j.ijhydene.2012.08.078.
[26] Falcão RB, Dammann EDCC, Rocha CJ, Ichikawa RU, Durazzo M, Martinez LG, Leal Neto RM. Synthesis of TiFe compound from ball milled TiH_2 and Fe powders mixtures. Mater Sci Forum 2014;802:61–5. https://doi.org/10.4028/www.scientific.net/MSF.802.61.
[27] Emami H, Edalati K, Matsuda J, Akiba E, Horita Z. Hydrogen storage performance of TiFe after processing by ball milling. Acta Mater 2015;88:190–5. https://doi.org/10.1016/j.actamat.2014.12.052.
[28] Falcão RB, Dammann EDCC, Rocha CJ, Durazzo M, Ichikawa RU, Martinez LG, Botta WJ, Lela Neto RM. An alternative route to produce easily activated nanocrystalline TiFe powder. Int J Hydrogen Energy 2018;43:16107–16. https://doi.org/10.1016/j.ijhydene.2018.07.027.
[29] Jurczyk M, Jankowska E, Makowiecka M, Wieczorek I. Electrode characteristics of nanocrystalline TiFe-type alloys. J Alloy Comp 2003;354:6–9. https://doi.org/10.1016/S0925-8388(02)01347-6.
[30] Zaluski L, Tessier P, Ryan DH, Doner CB, Zaluska A, Ström-Olsen JO, Trudeau ML, Schulz R. Amorphous and nanocrystalline Fe–Ti prepared by ball milling. J Mater Res 1993;8:3059–68. https://doi.org/10.1557/JMR.1993.3059.
[31] Abe M, Kuji T. Hydrogen absorption of TiFe alloy synthesized by ball milling and post-annealing. J Alloy Comp 2007;446–447:200–3. https://doi.org/10.1016/j.jallcom.2006.12.063.
[32] Aoki K, Aoyagi H, Memezawa A, Masumoto T. Effect of ball milling on the hydrogen absorption rate of FeTi and Mg_2Ni compounds. J Alloy Comp 1994;203:10–2. https://doi.org/10.1016/0925-8388(94)90704-8.
[33] Aoyagi H, Aoki K, Masumoto T. Effect of ball milling on hydrogen absorption properties of FeTi, Mg_2Ni and $LaNi_5$. J Alloy Comp 1995;231:804–9. https://doi.org/10.1016/0925-8388(95)01721-6.
[34] Jung CB, Lee KS. Electrode characteristics of metal hydride electrodes prepared by mechanical alloying. J Alloy Comp 1997;253–254:605–8. https://doi.org/10.1016/S0925-8388(96)03044-7.
[35] Novakova AA, Agladze OV, Sveshnikov SV, Tarasov BP. Supersaturated solid solutions and metastable phases formation through different stages of mechanical alloying of FeTi. Nanostructured Mater 1998;10:365–74. https://doi.org/10.1016/S0965-9773(98)00077-4.
[36] Chiang CH, Chin ZH, Perng TP. Hydrogenation of TiFe by high-energy ball milling. J Alloy Comp 2000;307:259–65. https://doi.org/10.1016/S0925-8388(00)00827-6.
[37] Delogu F, Cocco G. Compositional effects on the mechanochemical synthesis of Fe-Ti and Cu-Ti amorphous alloys by mechanical alloying. J Alloy Comp 2003;352:92–8. https://doi.org/10.1016/S0925-8388(02)01109-X.
[38] Jankowska E, Makowiecka M, Jurczyk M. Nickel-metal hydride battery using nanocrystalline TiFe-type hydrogen storage alloys. J Alloy Comp 2005;404–406:691–3. https://doi.org/10.1016/j.jallcom.2004.09.084.
[39] Vega LER, Leiva DR, Leal Neto RM, Silva WB, Silva RA, Ishikawa TT, Kiminami CS, Botta WJ. Mechanical activation of TiFe for hydrogen storage by cold rolling under inert atmosphere. Int J Hydrogen Energy 2018;43:2913–8. https://doi.org/10.1016/j.ijhydene.2017.12.054.
[40] Manna J, Tougas B, Huot J. Mechanical activation of air exposed TiFe + 4 wt% Zr alloy for hydrogenation by cold rolling and ball milling. Int J Hydrogen Energy 2018;43:20795–800. https://doi.org/10.1016/j.ijhydene.2018.09.096.
[41] Edalati K, Matsuda J, Iwaoka H, Toh S, Akiba E, Horita Z. High-pressure torsion of TiFe intermetallics for activation of hydrogen storage at room temperature with heterogeneous nanostructure. Int J Hydrogen Energy 2013;38:4622–7. https://doi.org/10.1016/j.ijhydene.2013.01.185.
[42] Edalati K, Matsuda J, Yanagida A, Akiba E, Horita Z. Activation of TiFe for hydrogen storage by plastic deformation using groove rolling and high-pressure torsion: similarities and differences. Int J Hydrogen Energy 2014;39:15589–94. https://doi.org/10.1016/j.ijhydene.2014.07.124.
[43] Saito T. Magnetic properties of Ti-Fe alloy powders prepared by mechanical grinding. J Alloy Comp 2004;364:113–6. https://doi.org/10.1016/S0925-8388(03)00532-2.
[44] Suryanarayana C. Mechanical alloying and milling. Prog Mater Sci 2001;46:1–184. https://doi.org/10.1016/S0079-6425(99)00010-9.
[45] Lü L, Lai MO. Mechanical alloying. Kluwer Academic Publishers; 1998.
[46] Berdonosova EA, Klyamkin SN, Zadorozhnyy VY, Zadorozhnyy MY, Geodakian KV, Gorshenkov MV, Kaloshkin SD. Calorimetric study of peculiar hydrogenation behavior of nanocrystalline TiFe. J Alloy Comp 2016;688:1181–5. https://doi.org/10.1016/j.jallcom.2016.07.145.
[47] Sandrock GD, Goodell PD. Surface poisoning of $LaNi_5$, FeTi and (Fe,Mn)Ti by O_2, CO and H_2O. J Less-Common Met 1980;73:161–8. https://doi.org/10.1016/0022-5088(80)90355-0.
[48] Williams M, Lototsky MV, Davids MW, Linkov V, Yartys VA, Solberg JK. Chemical surface modification for the improvement of the hydrogenation kinetics and poisoning resistance of TiFe. J Alloy Comp 2011;509:S770–4. https://doi.org/10.1016/j.jallcom.2010.11.063.
[49] Barkhordarian G, Klassen T, Bormann R. Kinetic investigation of the effect of milling time on the hydrogen sorption reaction of magnesium catalyzed with different Nb_2O_5 contents. J Alloy Comp 2006;407:249–55. https://doi.org/10.1016/j.jallcom.2005.05.037.
[50] Khawam A, Flanagan DR. Solid-state kinetic models: basics and mathematical fundamentals. J Phys Chem B 2006;110:17315–28. https://doi.org/10.1021/jp062746a.
[51] Pan Y-B, Wu Y-F, Li Q. Modeling and analyzing the hydriding kinetics of Mg-$LaNi_5$ composites by Chou model. Int J Hydrogen Energy 2011;36:12892–901. https://doi.org/10.1016/j.ijhydene.2011.06.145.
[52] Pang Y, Li Q. A review on kinetic models and corresponding analysis methods for hydrogen storage materials. Int J Hydrogen Energy 2016;41:18072–87. https://doi.org/10.1016/j.ijhydene.2016.08.018.
[53] Chou K-C, Li Q, Lin Q, Jiang LJ, Xu K-D. Kinetics of absorption and desorption of hydrogen in alloy powder. Int J Hydrogen Energy 2005;30:301–9. https://doi.org/10.1016/j.ijhydene.2004.04.006.
[54] Chou KC, Xu K. A new model for hydriding and dehydriding reactions in intermetallics. Intermetallics 2007;15:767–77. https://doi.org/10.1016/j.intermet.2006.10.004.
[55] Luo Q, An XH, Pan YB, Zhang X, Zhang JY, Li Q. The hydriding kinetics of Mg-Ni based hydrogen storage alloys: a comparative study on Chou model and Jander model. Int J Hydrogen Energy 2010;35:7842–9. https://doi.org/10.1016/j.ijhydene.2010.05.073.

[56] Wu G, Zhang J, Li Q, Chou K. A new model to describe absorption kinetics of Mg-based hydrogen storage alloys. Int J Hydrogen Energy 2011;36:12923–31. https://doi.org/10.1016/j.ijhydene.2011.07.026.
[57] Jander W. Reaktionen im festen Zustande bei höheren Temperaturen. I. Mitteilung. Reaktionsgeschwindigkeiten endotherm verlaufender Umsetzungen. Z Anorg Allg Chem 1927;163:1–30.
[58] Lv P, Guzik MN, Sartori S, Huot J. Effect of ball milling and cryomilling on the microstructure and first hydrogenation properties of TiFe+4 wt.% Zr alloy. J Mater Res Technol 2019;8(2):1828–34. https://doi.org/10.1016/j.jmrt.2018.12.013.
[59] Lv P, Liu Z, Dixit V. Improved hydrogen storage properties of TiFe alloy by doping (Zr+2V) additive and using mechanical deformation. Int J Hydrogen Energy 2019;44:27843–52. https://doi.org/10.1016/j.ijhydene.2019.08.249.